First Micromachined Silicon Load Cell for Loads up to 1000 kg

Henk Wensink, Meint J. de Boer, Remco J. Wiegerink, Robert A.F. Zwijze, Miko C. Elwenspoek
MESA Research Institute, University of Twente, P.O.Box 217, 7500 AE Enschede,
The Netherlands, Fax: x31-53-4893343, Email: H.Wensink@tn.utwente.nl

ABSTRACT

In this paper, a bulk micromachined silicon load cell is presented, designed for loads up to 1000 kg. ANSYS simulations were used to determine the load cell dimensions and strain gauge positions. The load cell consists of two parts, which are bonded to each other using Low Temperature Silicon Direct Bonding processes (LTSDB). To isolate the membrane with the sensors from lateral displacements within the load cell (e.g. expansion due to compression) thin silicon springs are incorporated in the design. To make these springs, a cryogenic RIE process with a high selectivity for resist was developed. A special housing was developed to apply a homogeneous load to the load cell. The sensor was successfully tested with loads up to 1000 kg using poly-silicon strain gauges.

Keywords: Force sensor, cryogenic RIE etching, Silicon Direct Bonding.

INTRODUCTION

Load cells are force sensors, which are used in weighing equipment. Most conventional load cells for loads of 1000 kg or more are made from steel or aluminium. When a load is applied, the metal part of the load cell deforms, which is measured by resistive strain gauges. To minimise hysteresis and creep, expensive materials and fabrication techniques have to be used. It is advantageous to make a load cell of silicon because in contrast to metals, it does not suffer from hysteresis and creep. Another advantage of silicon is that standard micromachining techniques can be used and accurate micromachined resonant strain gauges can easily be integrated in the design.

DESIGN AND OPERATION

The basic design of the load cell consists of a silicon membrane that is deformed while the load is carried by bulk silicon. Strain gauges on the membrane measure the resulting strain, which indicates the amount of load. An important design condition is that non-linear deformations of the (steel) housing may not influence the measurements. We designed a load cell consisting of two silicon wafers bonded to each other (Figure 1). The strain gauges are placed on a membrane (30µm thick) in the middle of the load cell. The frame of the load cell is a bearing block, which carries the complete load. In the centre at the bottom of the lid (top wafer), there is a small mesa which connects the lid to the membrane. The outline of the load cell is approximately 8 x 8 mm and its height 0.7 mm.

When a load is applied, the bearing block is compressed in the z direction, acting like a stiff spring. This results in a downward displacement of the lid. The membrane is also displaced downwards, but not as much as the lid (because its connection to the bearing block lies lower). The mesa will push the membrane down and make it

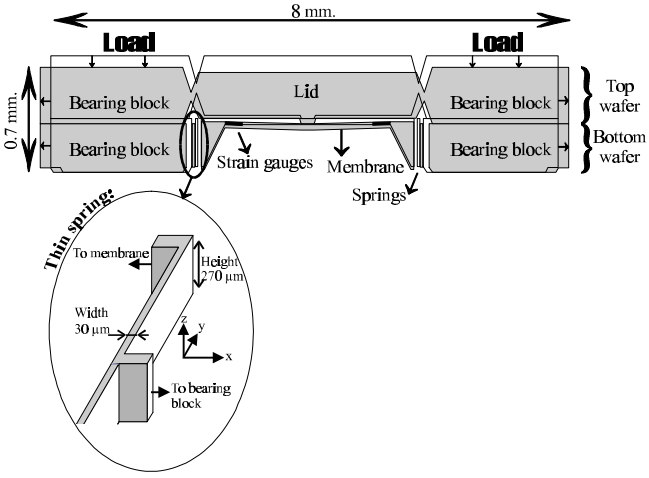

Figure 1. A cross section of a loaded load cell with a blow up of a thin spring.

bend; the strain sensors measure the induced strain. When a load is applied, the bearing block will not only be compressed in the z-direction but it also expands in the x and y direction. The effect of this expansion on the membrane was simulated using the finite element program ANSYS 5.3 [1]. It showed that it causes additional bending of the membrane, thus disturbing the strain measurement. To prevent this, the membrane is suspended to the bearing block by thin springs (see blow up in Figure 1) to isolate it from the expansion. Furthermore the springs reduce the effect on the membrane of other movements in the lateral direction,

such as non-linear displacements like creep and hysteresis from the steel housing of the load cell.

There are two design conditions for the springs; they must be stiff in the z-direction and weak in the lateral direction. The spring design however is also restricted by the load cell dimensions and technological constraints. The height is limited by the wafer thickness, 270 μm in our case. The width is restricted by the fact that electrical leads are necessary on top of the springs to connect the strain gauges; 30 μm is enough. The length is restricted by the width of the membrane; a single spring becomes 1150 μm long. Simulations show that only 1.2% of the strain on the membrane is caused by the lateral displacement of the bearing block. The other load cell dimensions are designed such that the strain in any place in the silicon never exceeds 1%. However, the dimensions of the bearing block are chosen such that a steel component of the same size can stand the maximum load (so we can use a steel housing). With an area of 32 mm^2, the stress of the bearing block will be 0.2 GPa at the most. The operation of the load cell was verified by finite element analysis (ANSYS 5.3) to locate the position of the accurate resonant strain gauges (they can be used in the future, piezoresistive strain gauges are used in this first prototype). For optimal sensitivity, the resonant strain gauge [2] must be placed at the position where the strain is $|10^{-5}|$ at maximum load (Figure 2).

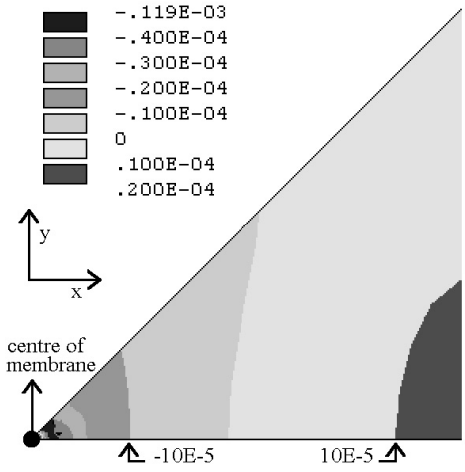

Figure 2. ANSYS plot of the strain in x direction on the membrane, showing 1/8 of the membrane (at maximum load).

FABRICATION

In Figure 3 the process scheme of the bulk micromachined load cell is presented. For the fabrication of the structures in the top wafer, simple compensation structures [3] were used to protect convex corners from underetching in KOH. For fabrication of the bottom

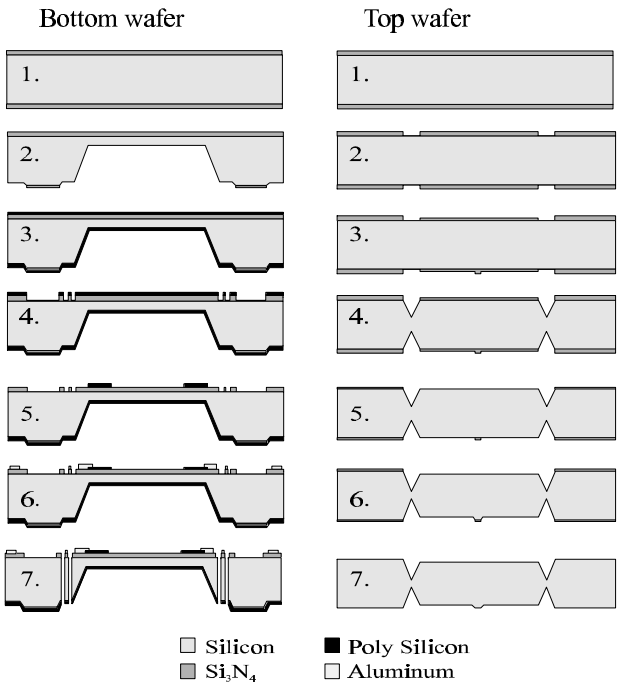

Figure 3. Fabrication scheme of the load cell.

wafer, 1μm low stress LPCVD nitride is deposited and is used as mask material for KOH etching (step 1) and as protection for the silicon bond surface. After patterning the nitride layer on the backside of the wafer with RIE, a membrane with a thickness of 30 μm is etched in KOH (step 2). Also a mesa structure with a height of 10 μm is etched on the backside of the wafer to avoid contact of the thin springs with the housing during operation. In step 3 poly-silicon is deposited. Poly-silicon is used as a mask material to etch nitride in 50% HF (step 4) and as the material for the strain gauges. In step 5 the poly-silicon strain gauges are patterned and etched by RIE. In step 6 aluminium is deposited for metalisation and the layer is patterned by lift-off techniques. In step 7 springs are etched with a cryogenic RIE process using SF_6/O_2 plasma chemistry.

Low Temperature Silicon Direct Bonding

To complete the load cell, the two wafers are connected by Low Temperature Silicon Direct Bonding (LTSDB) using a bonding temperature of 450°C. This low temperature is required to avoid damage to the aluminium metalisation and poly-silicon strain gauges (standard direct bonding uses an anneal temperature of 1100 °C). To achieve a low temperature bond, the wafer

surface has to be made hydrophilic by creating a thin native oxide layer on the silicon bond surface [4, 5]. Two oxidation procedures were tested, these procedures were preceded by a wafer clean in fuming HNO_3 and a rinse in demiwater. For comparison, we also bonded wafers without an extra oxidation. The two oxidation procedures are:

1. PE oxygen plasma using a Nanotech Plasmaprep 100 system; 1 min. 120 Watts, 55 sccm O_2, 150 °C, 2 mbar [6, 7].
2. 1% HF dip, 60 sec., followed by 100% HNO_3, 10 min. [8, 9].

After one of these treatments, the wafers are rinsed and dried by spinning and prebonded. Finally, they are annealed at 450 °C for 1 hour. The bond quality was verified by the razorblade method [4, 5], which uses a thin blade (40μm) to create a gap between the wafers. The bond energy can then be calculated from the gap length. The results are listed in Table 1.

Table 1: Low temperature bond quality

Treatment:	Bond energy: [J/m^2]
PE O_2 plasma	1.07
100% HNO_3 dip	0.34
no extra treatment	0.69

It appears that the Plasma Enhanced O_2 plasma gives the strongest bond and is sufficient for a reliable operation of the load cell. A good bond can only be made with very clean and smooth surfaces. Therefore, during of the fabrication of the wafers the silicon bondsurface is protected by a nitride layer for as long as possible. We observed that this layer has to be removed by using wet chemical etching of HF. Stripping the nitride layer with RIE creates a rough bondsurface and thereby reduces the bondstrength.

Cryogenic RIE SF_6/O_2

As motivated in the section design and operation the load cell requires thin springs for a proper operation. To realise these thin springs we used cryogenic RIE SF_6/O_2 plasma chemistry [10]. The advantages of this technique are; a high etch rate for silicon (up to 8 μm/min) which is indispensable for wafer through etching, a great freedom in mask design because the etched structures are not restricted by crystallic planes in the silicon, and different mask materials (metal, SiO_2, SiN, photoresist) can be applied. Mask materials like thermal SiO_2 and SiN make use of a high process temperature and this will damage the poly-silicon strain gauges and/or the aluminium metalisation. This means that only mask materials like photoresist and PVD of metals using low temperature can be used here. Another process demand is that fragile springs should be made at end of the process scheme of the bottom wafer. Because once the springs are made by creating holes in the wafer, standard lithography is not possible anymore (see Figure 3).

First we studied a Cr-mask and observed unwanted structuring problems. These problems are caused by "grass" in the etched areas due to redeposition of the mask material. So, photoresist is the only mask material left. The etch results of using photoresist of Shipley as mask material were promising, but the etchrate of photoresist was to high (selectivity of 100).

To improve the selectivity we developed an optimzation guideline for anisotropic etching of silicon (see Figure 4). In order to understand this guideline it is useful to explain in brief what is exactly meant by cryogenic RIE SF_6/O_2 plasma. In such a plasma F radicals are created from SF_6 for the spontaneous chemical etching of the

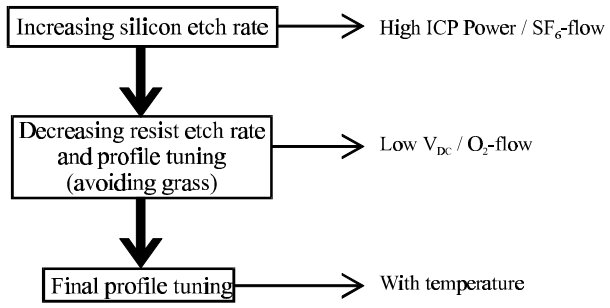

Figure 4. Optimization guideline for cryogenic RIE etching.

silicon forming volatile SiF_4. The O radicals are created from O_2 to passivate the silicon surface with SiO_xF_y, which blocks the etching. However, the SF_6 also produces SF_5^+ ions, which etch the SiO_xF_y layer thereby forming volatile SiO_xF_y species. The sidewalls of the etching structures are not exposed to ion bombardment and will be covered by the blocking layer. But the bottom of the structure is exposed to ion bombardment, which removes the blocking layer so etching can proceed, hence the process is directional. In the cryogenic process the substrate to be etched is cooled to temperatures as low as 150K. This temperature is low enough to prevent reaction products from the silicon etching (i.e. SiF_4) to escape from the surface. The blocking layer is now a mixture of reaction products like SiF_4 and SO_xF_y. Only in the case that impinging ions remove this layer etching can proceed and once again the process is directional. The advantage of etching silicon at these low temperatures is

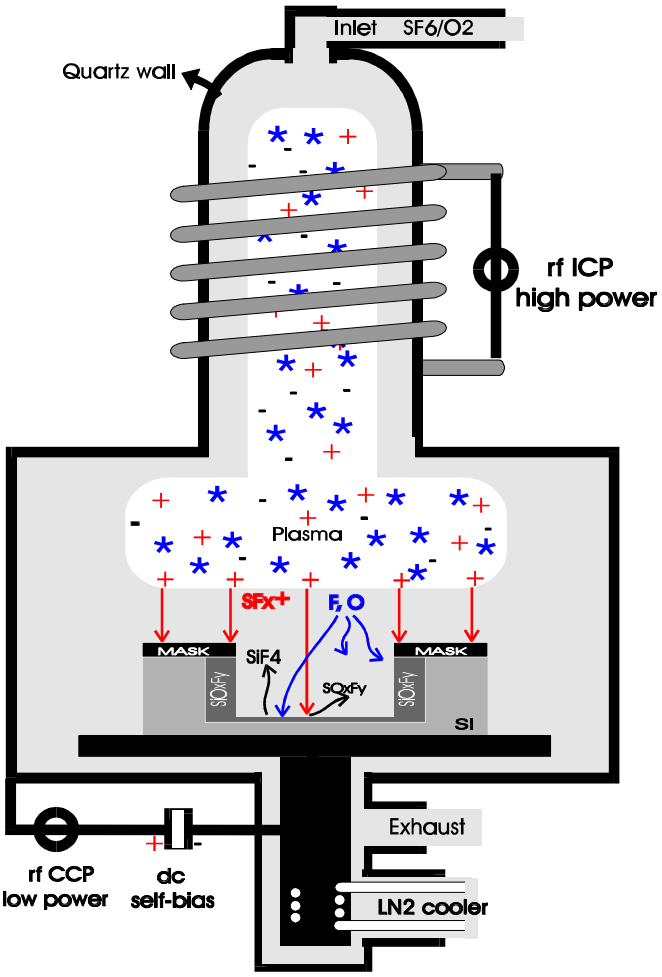

Figure 5. Schemetic representation of a modern commercial high density plasma etch tool.

that very low etchrates for photoresist can be achieved, because less oxygen is needed to form a blocking layer.

In Figure 5 a schematic representation of a modern commercial high-density plasma etch tool is shown (Oxford Plasmalab System 100 [11]). A high-power ICP source is used to generate a high density of radicals and a low-power CCP source is used to direct the ions with a predetermined kinetic energy to the sample to be etched. Especially the combination of a high radical-flux and a low-velocity ion-flux makes this system very flexible and therefore superior to most of the other plasma etch systems.

The parameters that can be adjusted for an optimal result are the SF_6 flow, oxygen content, ICP power, CCP power ($\Rightarrow$ self-bias), and temperature. During adjusting, the profile was kept fully anisotropic with the help of the Black Silicon Method (BSM [12]). The BSM gives us a guideline to trace the parameter setting where we can expect a good anisotropy; a kind of blueprint of the machine.

First, the silicon etch rate is maximized by increasing the SF_6-flow up to 120 sccm and ICP power up to 600 Watts keeping the process directional. The etchrate now is 5 µm/min with a load of 20% (3“ wafer). The temperature is fixed at -110 °C.

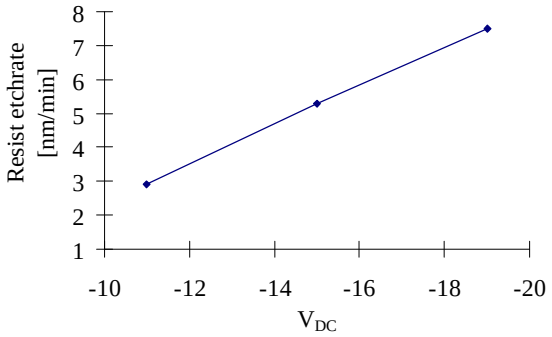

Figure 7. Resist etch rate versus the bias voltage V_{DC}.

Second we have to maximize the selectivity by decreasing the etchrate of photoresist. We observed that etchrate of photoresist is mainly determined by the O_2 content in the plasma. Therefore, the ICP power was not further increased to prevent a higher O_2 release from the quartz wall of the ICP source. Also the oxygen Mass Flow Controller (MFC) was closed, so the remaining O_2

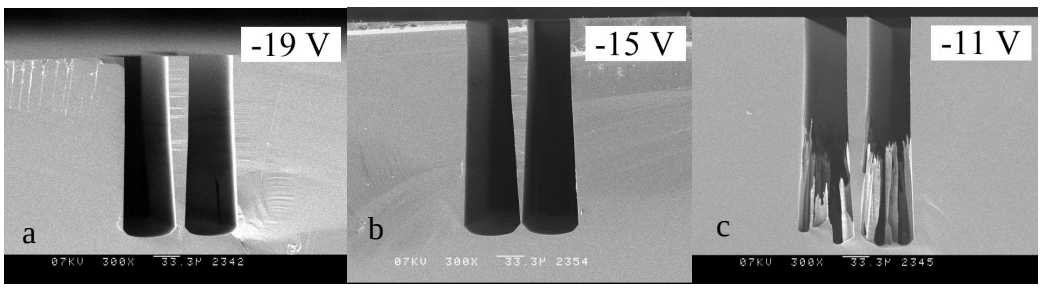

Figure 6. Trenches with variation in the bias voltage V_{DC}.

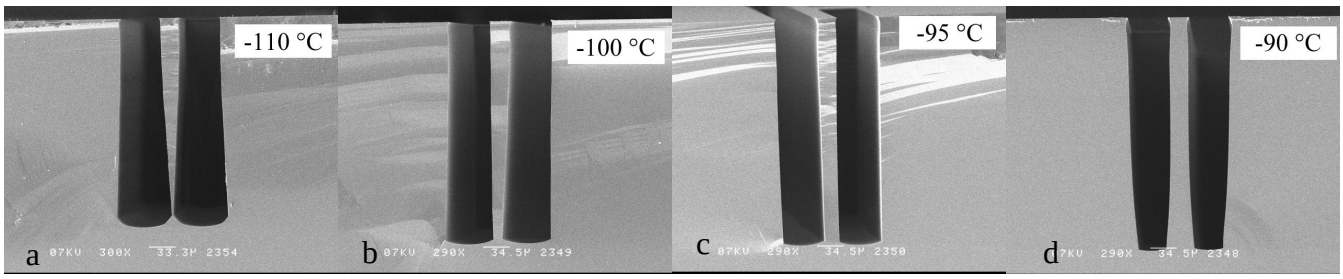

Figure 8. Influence of temperature on profile.

content originated from the quartz wall. To change the profile of the trenches, the CCP power is adjusted. This influences the bias-voltage (V_{DC}) and thereby the kinetic energy of the ions. The V_{DC} was lowered until grass appeared at the bottom of the trench (see Figure 6c). Grass must be avoided because it stops the etching process. We also observed that by decreasing the CCP power the etchrate of photoresist can be lowered down to 3 nm/min (Figure 7).

The last step of the guideline is to fine-tune the profile with the electrode temperature. In our case the profile was still negative so we increased the temperature up to -95 °C (see Figure 8). The selectivity is now in order of 1000. The average silicon etchrate is 3.3 micron/min and is a function of the aspect ratio of the trench and the loading of the wafer.

Another problem arises when a hole is etched through the wafer; the wafer temperature can not be controlled anymore. The heat transfer between the wafer and the LN_2-cooled electrode is controlled by helium gas flow (helium backside cooling, see Figure 9). So when a hole is etched the helium can escape and the no process control is possible anymore. To solve this problem, a polymer layer is applied on the backside of the wafer.

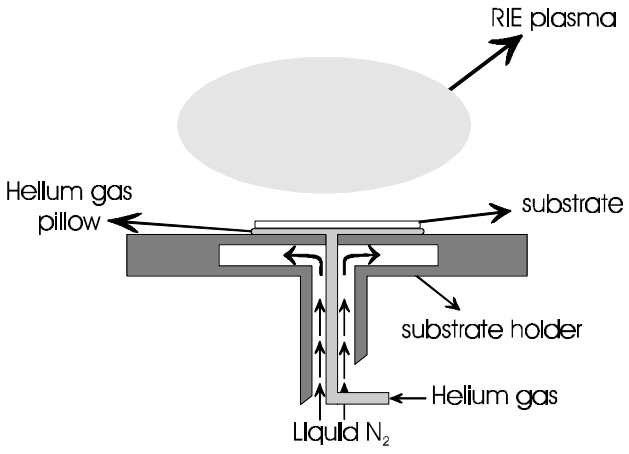

Figure 9. Helium backside cooling of the substrate.

MEASUREMENTS

So far, several load cell devices have successfully been fabricated. Two different configurations were made to apply a large force on the load cell (Figure 10). When using a solid steel block on top of the load cell, it will deform easily and tough the lid of the load cell. To avoid this, a hole was made in the steel block to make it fit perfectly on the bearing block of the silicon load cell

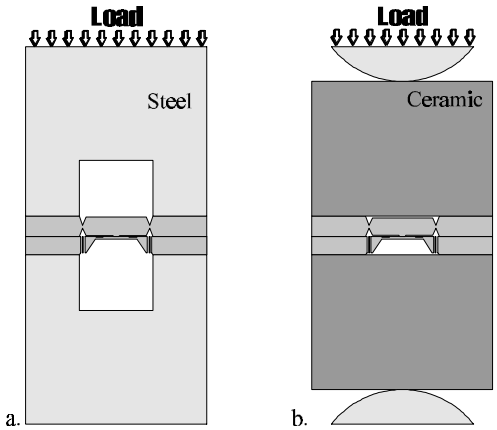

Figure 10. Two different configurations to apply the load to the load cell.

(Figure 10a.). However, it proved to be very difficult to make the steel with sufficient accuracy. Also, due to the different expansion (due to compression) and Young's modulus, the steel curves around the edges of the load cell causing large local stresses. This influences the measurements, and results in a premature fracture of the load cell. To prevent this, a ceramic block with a higher Young's modulus is used (Figure 10b). Now, the block will hardly deform and curve around the silicon, so it can be made solid. Also, a steel ball was added on top of the ceramic to ensure that the force is applied exactly in the middle of the ceramic block. The ceramic block was made long enough (2 cm) so that the point force on top of

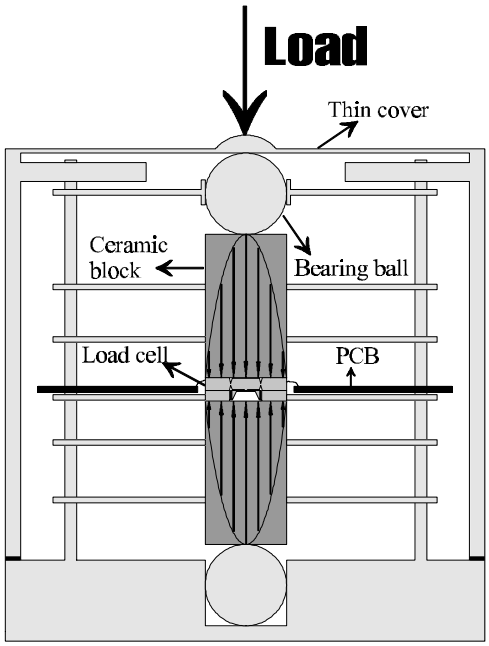

Figure 11. Cross section of the steel housing.

the ceramic is homogeneously distributed and applied to the load cell. A special steel housing was made to keep the load bearing components in place. (Figure 11). The housing takes care of the lateral forces and the device only measures perpendicular forces. The thin cover of the housing (0.5 mm) carries some amount of load, but calculations shows that this is only 0.05% at the maximum load. Another advantage of the closed housing (Figure 12) is that the poly-silicon sensors will be less influenced by local temperature differences (draft) and light intensity.

With this package we were able to test the load cell up to 1000 kg using poly-silicon strain gauges in a Wheatstone

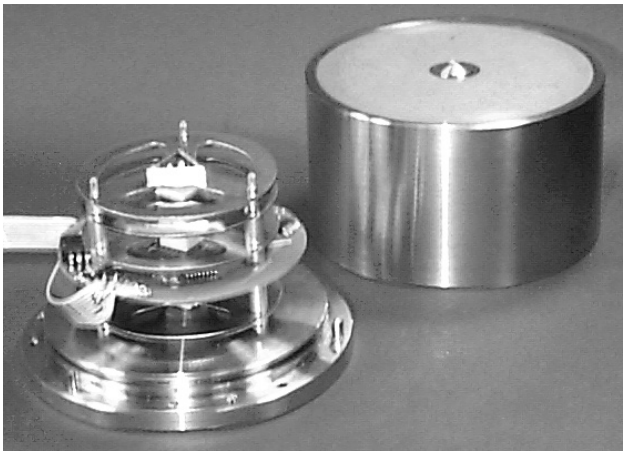

Figure 12. Photograph of the steel housing (open).

bridge configuration. A nano volt/micro ohm meter (HP-34420A) was used to measure the bridge output voltage and the supply voltage simultaneously and calculate the

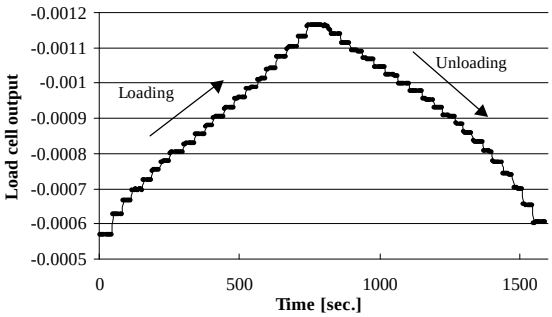

Figure 13. Load cell output versus time (every step represents a load increase or decrase of 50 kg).

ratio. In this way the influence of power supply variations is eliminated. Twenty weights of 50 kg were used to reach the maximum load, measurements are taken every 5 seconds. Figure 13 shows the measured output as a function of time, every step in the measurements represents a load increase or decrease of 50 kg. Figure 14 shows the average output for every load.

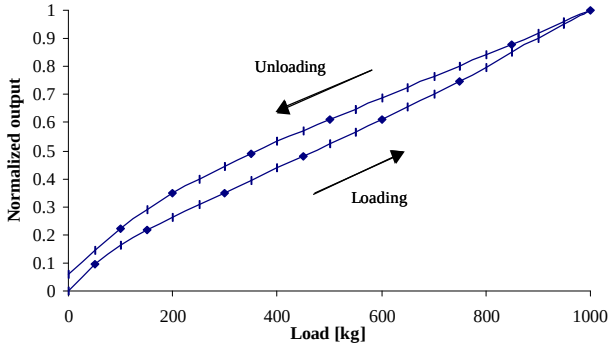

Figure 14. Normalized load cell output versus load.

DISCUSSION

The measurements show a bridge output of approximately $0.58 \cdot 10^{-3}$ at maximum load, which is in our system, equivalent to a strain of $2 \cdot 10^{-5}$. This is only twice as much as we expected and can easily be explained by a deviation in gauge factor of the strain gauges. Above 100 kg the output was almost linear, which can be expected when the membrane deflection is only 1 μm. However, up to 100 kg a relative large slope is observed. We suggest the following argumentation.

Without a load, the ceramic touches the silicon at only a few points. When a small load is applied, it is conducted through these points resulting in a very inhomogeneous load distribution. The effect of this on the load cell output is unpredictable, but will be relatively large at small loads. Once a large load is applied, the ceramic and/or silicon bends and more contact points are available to distribute the load. The higher zero load output after unloading originates partly from drift, but the system also suffers from creep. This can be caused by the steel components of the housing (e.g. when the steel ball is pressed, it no longer exerts a point force to the ceramic). Also, a lot of hysteresis is observed. We believe that this is caused by the lower horizontal expansion (due to the vertical compression) of the ceramic in comparison with the silicon. Due to this different expansion rate, the silicon grazes over the ceramic. Also, even the ceramic will slightly curve around the edges of the load cell. These effects result in an inhomogeneous load distribution, which will be different for loading and unloading.

This micromachined silicon load cell gives us the possibility to integrate the more accurate resonant strain gauges and additional electronics in the design. However, before it is useful to do so, the sensor has to be made less sensitive to inhomogeneous load distributions. This is improved when the ceramic is structured to fit perfectly on the load cell. However, even when it's possible to machine the ceramic at a sufficient accuracy, it will remain very difficult to place the ceramic with the same accuracy on the silicon load cell. Further research is directed to find a solution for the ceramic/silicon interface. We also investigate other load cell designs that are less sensitive to inhomogeneous load distributions.

CONCLUSIONS

A micromachined silicon load cell for loads up to 1000 kg was realised. KOH etching was used to define the major structure of the load cell. Essential elements in the design of the load cell are the thin springs. They make sure that any movement in the lateral direction, e.g. due to expansion of the bearing block, is not passed on to the membrane. For this prototype, the springs are made with anisotropic cryogenic RIE etching. Photo resist was used as a masking material, because of its compatibility with the other process steps. A new guideline was developed that increase the selectivity of resist to make the high springs possible. A polymer layer was applied as a backside protection, preventing the process to be disturbed once a hole was etched through the wafer. Low Temperature Silicon Direct Bonding procedures were used to bond the top and bottom wafer. The low temperature (450°C) prevents the aluminium connections and poly-silicon strain gauges from being damaged. Good bonds with a surface energy of more than 1 J/m^2 have been made at this temperature. The sensor was successfully tested with poly-silicon strain gauges up to 1000 kg in a special developed housing. Measurements still show hysteresis. This problem originates in the difficulty to apply the load homogeneously to the load cell. Future research is directed to find a solution for the silicon/ceramic interface. Also, alternative load cell designs are investigated which are less sensitive to inhomogeneous loads.

ACKNOWLEDGMENTS

This research was supported by the Dutch Technology Foundation (STW). The authors are grateful to M.T. Dijkstra for the ANSYS simulations, to H.V. Jansen for his contribution to the RIE process, to P.E. de Graaff and T.M.P.A. Bartels for their work on the housing and to J.W. Berenschot for technological advises.

REFERENCES

1. M.T.Dijkstra, graduate report TDM University of Twente, (1996).
2. H.A.C.Tilmans, thesis University of Twente, (1993).
3. H.L.Offereins, K.Kühl, H.Sandmaier, *Sensors and Actuators A*, 25-27, (1991), pp. 9-13.
4. Q.Y.Tong, U.Gösele, A Model of Low-Temperature Wafer Bonding And Its Applications, *J. Electrochem. Soc.*, Vol. 143, No. 5, (1996), pp. 1773-1779.
5. R.Stengl, T.Tan, U.Gösele, A Model for the Wafer Bonding Process, *Japanese Journal of Applied Physics*, Vol. 28, No. 10, (1989), pp. 1735-1741.
6. M.Wiemer, T.Geβner, K.Hiller, *Micro system Technologies '92*, ed. H.Reichl, (1992), pp. 65-75.
7. W.Kissenger, G.Kissenger, *Proceedings of the first international symposium on semiconductor wafer bonding: science, technology, and applications*, Phoenix, Arizona, (1991), pp. 73-81.
8. J.Jiao, D.Lu, B.Xiong, W.Wang, *Sensors and Actuators A*, 50, (1995), pp. 117-120.
9. A.Berthold, P.M.Sarro, P.J.French, M.J.Vellekoop, *Eurosensors X*, Vol.2, (1996), pp. 489-492.
10. H.V. Jansen, M.J. de Boer, R. Legtenberg, M.C. Elwenspoek, The black silicon method: a universal method for detemining the parameter setting of a fluorine-based reactive ion etcher in deep silicon trench etching with profile control, *J. of Micromech. Microeng.*, Vol. 5, (1995), pp.115-120.
11. Oxford Instruments, Plasma Technology, North End, Yatton, Bristol BS19 4AP, England, Tel. +44(1934)876444/833851, Fax +44(1934)834918.
12. H.V. Jansen, M.J. de Boer, H. Wensink, B. Kloeck, M.C. Elwenspoek, The black silicon method VIII: a study of the performance of etching silicon using SF_6/O_2-based chemistry with cryogenical wafer cooling and a high density ICP source, *Microelectronic Eng.*, Vol. 41-42, (to be publicised).